Diffusion Propagator Estimation Using Radial Basis Functions

Yogesh Rathi, Marc Niethammer, Frederik Laun, Kawin Setsompop, Oleg Michailovich, P. Ellen Grant, and C.-F. Westin

Abstract The average diffusion propagator (ADP) obtained from diffusion MRI (dMRI) data encapsulates important structural properties of the underlying tissue. Measures derived from the ADP can be potentially used as markers of tissue integrity in characterizing several mental disorders. Thus, accurate estimation of the ADP is imperative for its use in neuroimaging studies. In this work, we propose a simple method for estimating the ADP by representing the acquired diffusion signal in the entire q-space using radial basis functions (RBF). We demonstrate our technique using two different RBF's (generalized inverse multiquadric and Gaussian) and derive analytical expressions for the corresponding ADP's. We also derive expressions for computing the solid angle orientation distribution function (ODF) for each of the RBF's. Estimation of the weights of the RBF's is done by

Y. Rathi (✉) · C.-F. Westin
Brigham and Women's Hospital, Harvard Medical School, Boston, MA, USA
e-mail: yogesh@bwh.harvard.edu; westin@bwh.harvard.edu

M. Niethammer
University of North Carolina, Chapel Hill, NC, USA
e-mail: mn@cs.unc.edu

F. Laun
German Cancer Research Center, Heidelberg, Germany
e-mail: F.Laun@dkfz-heidelberg.de

K. Setsompop
Massachusetts General Hospital, Harvard Medical School, Boston, MA, USA
e-mail: kawin@nmr.mgh.harvard.edu

O. Michailovich
University of Waterloo, Waterloo, ON, Canada
e-mail: olegm@uwaterloo.ca

P.E. Grant
Boston Children's Hospital, Harvard Medical School, Boston, MA, USA
e-mail: Ellen.Grant@childrens.harvard.edu

T. Schultz et al. (eds.), *Computational Diffusion MRI and Brain Connectivity*, Mathematics and Visualization, DOI 10.1007/978-3-319-02475-2_6,

enforcing positivity constraint on the estimated ADP or ODF. Finally, we validate our method on data obtained from a physical phantom with known fiber crossing of 45 degrees and also show comparison with the solid spherical harmonics method of Descoteaux et al. (Med Image Anal 2010). We also demonstrate our method on in-vivo human brain data.

1 Introduction

A popular dMRI acquisition technique is High Angular Resolution Diffusion Imaging (HARDI), which involves acquiring diffusion information for a single b-value (single shell) in several gradient directions uniformly spread on a sphere [16]. While this protocol allows for resolving the angular structure of the neural fibers, it does not provide information about the radial signal decay, which is sensitive to white matter anomalies [6].

To obtain accurate information about the neural architecture, diffusion spectrum imaging (DSI) was proposed by [17]. This high resolution technique requires upwards of 512 gradient directions and more than an hour to scan each subject (spatial resolution of 2 mm^3), which makes it impractical to use in clinical settings. Consequently, other imaging and analysis schemes have been proposed, namely, Hybrid Diffusion Imaging (HYDI) [18], Diffusion Propagator Imaging (DPI) [7], Diffusion Kurtosis Imaging (DKI) [9], CHARMED [2], NODDI [20], spherical polar Fourier basis [3, 10], MAP-MRI [12], spherical ridgelets [14] and high-order tensor models [4, 8]. Each of these techniques captures a different aspect of the underlying tissue geometry. Thus, the CHARMED and NODDI models utilize specific acquisition sequences to estimate the axon diameter distribution, while DKI uses low-to-medium b-values ($b < 3{,}000$) to obtain information about the non-Gaussian part of the diffusion process. The work of [18] on the other hand uses numerical computations to compute the propagator from measurements spread intelligently in the q-space, while DPI, spherical polar Fourier basis, and the spherical ridgelet methods extend the spherical representation of a single shell to multiple shells by adding a radial term to their basis functions. The method developed in [12] works by representing the diffusion propagator (and the diffusion signal) using Hermite polynomials. Although significantly different, our work is closest in spirit to the box-spline and Hermite polynomial method of [12, 19].

2 Our Contributions

In this work, we use radial basis functions, which are radially symmetric functions, for representing the diffusion data and computing the average diffusion propagator (ADP). Representing the diffusion data using radially symmetric RBF's reduces the

problem of computing the 3D Fourier transform of the diffusion signal to a simple 1D Fourier transform of the RBF. This in turn leads to a very simple expression for computing the Fourier transform of the diffusion signal. Given that the acquired diffusion signal $E(\mathbf{q})$ in q-space is related to the average diffusion propagator via the Fourier transform, the radial basis functions thus become a natural choice for computing the ADP. Further, these functions have been used quite successfully in other fields of research involving interpolation in high-dimensional spaces [5].

The novel part of our work lies in using radial basis functions to represent the diffusion data in the entire q-space and deriving analytical expressions for computing the corresponding ADP for two different RBF's. We also derive closed form expressions for computing the solid angle ODF and validate our methods on a physical phantom data set with a known crossing angle, apart from showing some in-vivo results on human brain data.

3 Data Representation Using Radial Basis Functions (RBF)

The idea behind data representation using radial basis function is to express a continuous function by means of a linear combination of radially symmetric basis functions centered around the given data points. Given a radial basis function $\phi(r) = \phi(\|\boldsymbol{x}\|)$, $\mathbf{x} \in R^d$ and a sampling of the continuous function $f(\boldsymbol{x})$ as a set of N data/location pairs $\{(\boldsymbol{x}_i, f_i)\}$ (with distinct locations $\boldsymbol{x}_i$), its radial basis function reconstruction is given by: $\hat{f}(\boldsymbol{x}) = \sum_{i=0}^{N} w_i \phi(\|\boldsymbol{x} - \boldsymbol{x}_i\|)$, where the interpolation weights are computed by solving the linear system induced by

$$f_j = \sum_{i=0}^{N} w_i \phi(\|\boldsymbol{x}_j - \boldsymbol{x}_i\|), \tag{1}$$

which can be written in matrix form as

$$w_i = (A_{ji})^{-1} f_j, \quad A_{ji} = \phi(\|\boldsymbol{x}_j - \boldsymbol{x}_i\|). \tag{2}$$

To estimate the ADP, we are interested in radial basis functions that can be easily Fourier transformed. In this work, we chose the following two functions as candidates for RBF's [5]: the Gaussian and the generalized inverse multiquadric:

$$\phi_g(r) = e^{-c^2 r^2}, \quad \phi_{gm}(r) = \frac{1}{(r^2 + c^2)^{\mu+1}}, \quad c > 0.$$

These choices are driven by the fact that all these functions are (conditionally) positive definite leading to a unique solution for w_i [5].

3.1 Application to Diffusion MRI

Diffusion MRI measurements are assumed to have antipodal symmetry, i.e., $f(\boldsymbol{x}) = f(-\boldsymbol{x})$. This feature of dMRI data can be accounted for in our RBF approach in the following two ways: (i) the number of measuremtents can artifically be doubled, i.e., for every pair $(\boldsymbol{x}_i, f_i)$ add a pair $(-\boldsymbol{x}, f_i)$, (ii) the symmetry can be taken into account directly in the interpolation procedure. This paper follows the latter route, since explicitly keeping the antipodal pairing clarifies the Fourier relations in Sect. 3.2. The RBF expansion for the antipodal case may be written as

$$f_j = \sum_{i=0}^{N} w_i \left[\phi(\|\boldsymbol{x}_j - \boldsymbol{x}_i\|) + \phi(\|\boldsymbol{x}_j + \boldsymbol{x}_i\|)\right]. \tag{3}$$

For this to hold, $w_i = w_j$ if $\boldsymbol{x}_i = -\boldsymbol{x}_j$.

3.2 Estimating the ADP with Radial Basis Functions

The diffusion measurements are expressed by radial basis functions as a continuous function $f(\boldsymbol{x})$. The ADP is then given by its Fourier transform. Since the RBF representation is a simple linear combination, its Fourier transform is also given by a linear combination of the Fourier transforms of the individual basis functions. The Fourier transform of a radial basis function is also radially symmetric and may be computed using the Hankel transform [5]. As shown in [13], the n-dimensional Fourier transform of a radially symmetric function of n variables is related to the Hankel transform of order $\frac{n}{2} - 1$. Thus, given a radially symmetric RBF $\phi(r)$, its n-dimensional Fourier transform is also radially symmetric and is given by:

$$\Phi(k) = (2\pi)^{\frac{n}{2}} k^{-\frac{n}{2}+1} \mathscr{H}_{\frac{n}{2}-1}\left(r^{\frac{n}{2}}\phi(r)\right),$$

where the ν-th order Hankel transform $\mathscr{H}(\cdot)$ is defined as [13]

$$\mathscr{H}_\nu\left(f(r)\right) := \int_0^\infty r f(r) J_\nu(kr)\, dr,$$

where J_ν is the ν-th order Bessel function of the first kind. Note that, **the n-dimensional Fourier transform is only a function of the radial co-ordinate in the Fourier domain.**

For the Gaussian radial basis function the 3D Fourier transform is thus (see [1] for integral expressions)

$$\Phi_g(k) = (2\pi)^{\frac{3}{2}} \frac{1}{\sqrt{k}} \int_0^\infty e^{-c^2 r^2} r^{\frac{3}{2}} J_{\frac{1}{2}}(rk)\, dr = \left(\frac{\pi}{c^2}\right)^{\frac{3}{2}} e^{-\frac{k^2}{4c^2}},$$

and for the generalized inverse multiquadric it becomes

$$\begin{aligned}\Phi_{gm}(k) &= (2\pi)^{\frac{3}{2}} \frac{1}{\sqrt{k}} \int_0^\infty \frac{1}{(r^2+c^2)^{\mu+1}} r^{\frac{3}{2}} J_{\frac{1}{2}}(rk)\, dr, \\ &= (2\pi)^{\frac{3}{2}} \frac{1}{\sqrt{k}} c^{\frac{1}{2}-\mu} \left(\frac{k}{2}\right)^{\mu} \frac{1}{\Gamma(\mu+1)} K_{\frac{1}{2}-\mu}(kc) \\ &= (2\pi)^{\frac{3}{2}} \sqrt{\frac{c}{k}} K_{\frac{1}{2}}(kc), \quad \text{for } \mu = 0.\end{aligned}$$

where $K_\nu(\cdot)$ is the ν-th order modified Bessel function of the second kind and $\Gamma(\cdot)$ denotes the gamma function.

For representing the diffusion signal throughout q-space, the RBFs are centered at each of the data points at which the measurements are available. Thus, a translation of the RBF's should be taken into account while computing the Fourier transform $\mathscr{F}$ of the q-space diffusion signal. A translation of a basis function causes (according to the Fourier shift theorem) a phase shift of its Fourier transform, i.e., $\mathscr{F}(f(\boldsymbol{x})) = F(\boldsymbol{k}), \quad \rightarrow \quad \mathscr{F}(f(\boldsymbol{x}+\boldsymbol{a})) = e^{i\boldsymbol{a}^T\boldsymbol{k}} F(\boldsymbol{k})$. Due to the antipodal symmetry assumed for diffusion weighted imaging, i.e., $f(\boldsymbol{x}) = f(-\boldsymbol{x})$ we have

$$\mathscr{F}(f(\boldsymbol{x}+\boldsymbol{a}) + f(\boldsymbol{x}-\boldsymbol{a})) = 2\cos(\boldsymbol{a}^T\boldsymbol{k}) F(\boldsymbol{k})$$

and thus the 3D Fourier transforms for an antipodal basis pair for the Gaussian RBF and the generalized inverse mutliquadric RBF becomes

$$\Phi_g^{\boldsymbol{a}}(\boldsymbol{k}) = 2\left(\frac{\pi}{c^2}\right)^{\frac{3}{2}} e^{-\frac{\|\boldsymbol{k}\|^2}{4c^2}} \cos(\boldsymbol{a}^T\boldsymbol{k}), \tag{4}$$

$$\Phi_{gm}^{\boldsymbol{a}}(\boldsymbol{k}) = (2\pi)^{\frac{3}{2}} \sqrt{\frac{c}{\|\boldsymbol{k}\|}} K_{\frac{1}{2}}(\|\boldsymbol{k}\|c) \cos(\boldsymbol{a}^T\boldsymbol{k}), \quad \text{for } \mu = 0. \tag{5}$$

Finally, from coefficients estimated in (3), the ADP using each of the RBF's can be computed using the following expressions:

$$P_g(\boldsymbol{r}) = \sum_{i=0}^{N} w_i \Phi_g^{\boldsymbol{x}_i}(\boldsymbol{r}) = 2\sum_{i=1}^{N} w_i \left(\frac{\pi}{c^2}\right)^{\frac{3}{2}} e^{-\frac{\|\boldsymbol{r}\|^2}{4c^2}} \cos({\boldsymbol{x}_i}^T\boldsymbol{r}), \tag{6}$$

$$P_{gm}(\boldsymbol{r}) = \sum_{i=0}^{N} w_i \Phi_{gm}^{\boldsymbol{x}_i}(\boldsymbol{r}) = 2\sum_{i=1}^{N} w_i\, (2\pi)^{\frac{3}{2}} \sqrt{\frac{c}{\|\boldsymbol{r}\|}} K_{\frac{1}{2}}(\|\boldsymbol{r}\|c) \cos({\boldsymbol{x}_i}^T\boldsymbol{r}), \tag{7}$$

where the expression for $P_{gm}(\boldsymbol{r})$ was computed for $\mu = 0$. A closed form expression for the ADP using the generalized inverse multiquadric can also be computed for any $\mu \geq -\frac{1}{2}$:

$$P^{\mu}_{gm}(\boldsymbol{r}) = 2^{(1-\mu)}\,(2\pi)^{\frac{3}{2}} \sum_{i=1}^{N} \frac{w_i}{\Gamma(\mu+1)} \left(\frac{\|\boldsymbol{r}\|}{c}\right)^{(\mu-0.5)} K_{\frac{1}{2}-\mu}(\|\boldsymbol{r}\|c)\cos(\boldsymbol{x_i}^T\boldsymbol{r}). \quad (8)$$

3.3 Computing the Orientation Distribution Function (ODF)

The orientation distribution function (ODF) can be computed using the ADP [17] by evaluating the integral $\Psi(\boldsymbol{u}) = \int_0^{\infty} P(k\boldsymbol{u})k^2\,dk$, where $\boldsymbol{u}$ is a unit vector on $\mathscr{S}^2$ and k is the radial co-ordinate. For the Gaussian RBF this integral can be evaluated analytically as:

$$\Psi_g(\boldsymbol{u}) = 8(\pi c)^2 \sum_{i=0}^{\infty} w_i \left(\frac{1}{2c^2} - (\boldsymbol{x_i}^T\boldsymbol{u})^2\right) \exp\left(-(c\boldsymbol{x_i}^T\boldsymbol{u})^2\right),$$

and for the generalized inverse multiquadric, the ODF (solid-angle version) is given by:

$$\begin{aligned}\Psi_{gm}(\boldsymbol{u}) &= 2^{(1-\mu)}\,(2\pi)^{\frac{3}{2}} \sum_{i=0s}^{N} \frac{w_i}{\Gamma(\mu+1)} c^{(\mu-0.5)} \int_0^{\infty} k^{\mu+1.5} K_{0.5-\mu}(kc)\cos(k\boldsymbol{x}_i^T\boldsymbol{u})dk,\\ &= (4\pi)^{\frac{3}{2}}\, c^{-3} \sum_{i=0}^{N} \frac{w_i \Gamma(1.5)\Gamma(\frac{2\mu+1}{2})}{\Gamma(\mu+1)} F\left(\frac{3}{2}, \frac{2\mu+1}{2}; \frac{1}{2}, \frac{-(\boldsymbol{x}_i^T\boldsymbol{u})^2}{c^2}\right), \quad \mu > -1\end{aligned}$$

where F is the Gauss-hypergeometric function.

3.4 Estimation Procedure

Estimation of the coefficients w_i in Eq. (3) can be done in a number of different ways. One of the simplest method is to estimate w_i by solving a linear system of equations with as many measurements as unknowns (w_i). Thus, $\boldsymbol{w} = A^{-1}\boldsymbol{f}$, where $\boldsymbol{f}$ is a vector of measurements acquired at various q-values, and the matrix A is as defined in Eq. (2). This method however, does not account for the fact that the diffusion propagator is positive. Thus, one could enforce this constraint while estimating the vector of weights $\boldsymbol{w}$. The cost function then becomes:

$$\min_{\boldsymbol{w}} \parallel A\boldsymbol{w} - \boldsymbol{f} \parallel^2, \text{ s.t. } B\boldsymbol{w} \geq 0,$$

where, the matrix B is computed from $P_g(\boldsymbol{r})$ or $P_{gm}(\boldsymbol{r})$ (Eq. 6) by choosing a particular value for the radius $\|r\|$. Alternatively, one could enforce this positivity constraint to ensure that the estimated ODF is also positive everywhere. In this case,

the matrix B is constructed using the expression for $\Psi_g(\boldsymbol{u})$ or $\Psi_{gm}(\boldsymbol{u})$. Notice that, in this case, one does not have to choose the radius parameter $\|r\|$. Estimation of $\boldsymbol{w}$ can now be done using quadratic programming by minimizing the cost function: $\min_{\boldsymbol{w}}(\boldsymbol{w}^T A^T A\boldsymbol{w} - 2\boldsymbol{f}^T A)$, s.t. $B\boldsymbol{w} \geq 0$.

4 Experiments

To test our method, we use data acquired from a physical phantom with a crossing angle of 45°. The spherical crossing phantom was built as given in [11] and data was acquired at five different b-values $b = \{1{,}000, 2{,}000, 3{,}000, 4{,}000, 5{,}000\}$. Each b-value shell consisted of 60 gradient directions, for a total of 300 diffusion acquisitions. The weights $\boldsymbol{w}$ were estimated using the quadratic cost function with the positivity constraint. Figure 1 shows the baseline and FA images of the phantom near the crossing angle. The acquisition was done at a spatial resolution of $2 \times 2 \times 7\,\text{mm}^3$ to get a better coverage of the crossing region.

Estimation of the weights $\boldsymbol{w}$ was done for two RBF's: (1) the Gaussian RBF and (2) the inverse multiquadric with $\mu = 0$. Figure 2 shows the estimated propagator in the crossing region by setting the following parameters: $c = 0.20, \|r\| = 0.20$ in $P_g(\boldsymbol{r})$ and $P_{gm}(\boldsymbol{r})$ (Eq. (6)) (positivity constraint was enforced to obtain positive ADP's).

The average crossing angle estimated for the ADP computed using the Gaussian RBF was $50.16° \pm 4.23°$, and for the generalized inverse multiquadric it was $52.75° \pm 5.02°$. Similarly, we also computed the ADP and the ODF using the solid spherical harmonics method (order $L = 6$) of [7]. The average angular crossing estimated using this method was $59.74° \pm 6.78°$ (which is an angular error of $14.74°$) (Fig. 3).

4.1 In-Vivo Results

We tested our method on in-vivo human brain data acquired with the following scan parameters: b-values of $\{250, 900, 2{,}000, 3{,}600, 5{,}600\}$ s/mm^2, with each b-value shell having $\{6, 60, 60, 60, 60\}$ gradient directions (a total of 246 gradient directions), spatial resolution of $2.5\,\text{mm}^3$ isotropic, TE = 130 ms, and TR = 10.6 s. Figure 4 shows the ADP computed using the Gaussian and the generalized inverse multiquadric RBF at $\|r\| = 0.2$. We should note that this value of $\|r\|$ does not correspond to the physical space in mm, but is the variable in Fourier domain for RBF functions $\Phi(\boldsymbol{r})$ placed at each data point. Further, we used $c = 0.2$ for the Gaussian RBF and $c = 2$ for the generalized inverse multiquadric. As can be seen in Fig. 4, the ADP for both RBF's looks quite similar with crossing fibers visible in the centrum semiovale.

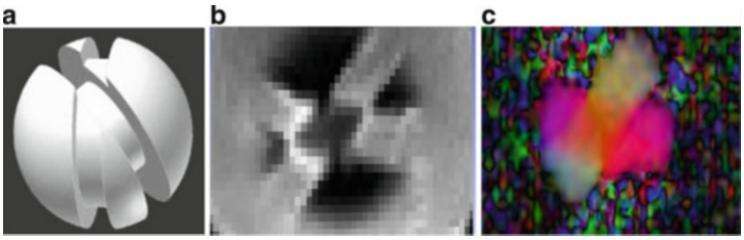

Fig. 1 Photographic, Baseline (b = 0) and fractional anisotropy (FA) images of a spherical phantom, where two fiber bundles cross at 45° angle. (**a**) Phantom. (**b**) Baseline (b = 0). (**c**) FA (zoomed)

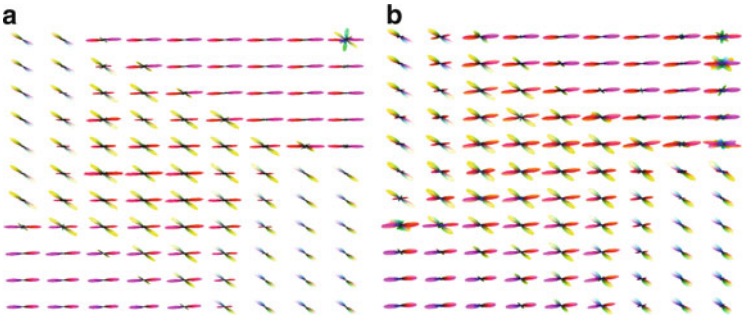

Fig. 2 Diffusion propagator (ADP) estimated using (**a**) Gaussian RBF. (**b**) Generalized inverse multiquadric with $\mu = 0$

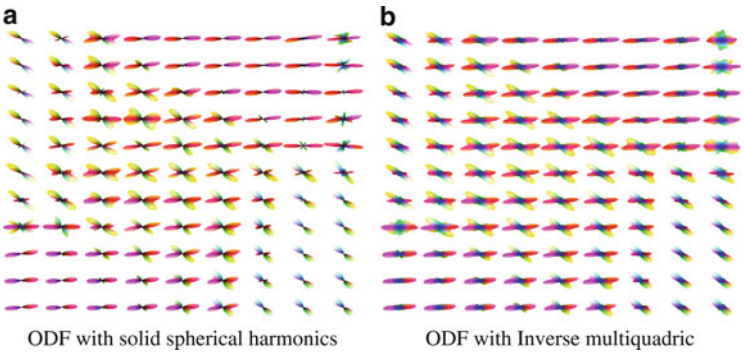

Fig. 3 ODF estimated using (**a**) Solid spherical harmonics (order $L = 6$) of [7]. (**b**) Generalized inverse multiquadric

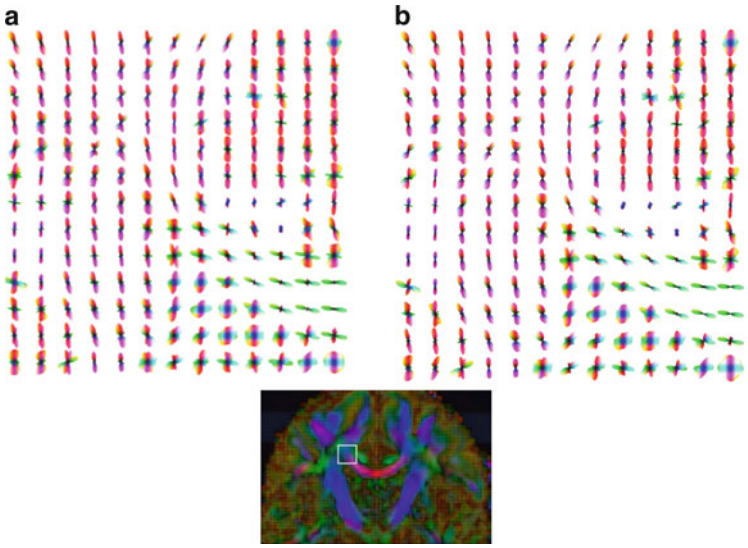

Fig. 4 ADP estimated using (**a**) Gaussian RBF and (**b**) Generalized inverse multiquadric for the *rectangular region* shown on a coronal color coded FA slice

5 Conclusion

In this work, we presented a first application of using radial basis functions for representing the diffusion data in the entire q-space as well derived closed form expressions for computing the average diffusion propagator (ADP). We derived analytical expressions for the ADP and ODF using two RBF's, namely, the Gaussian and the generalized inverse multiquadric. We showed some quantitative results on a physical phantom data set and compared our method with an existing state-of-the-art method of [7]. Our preliminary results on phantom and in-vivo data shows that the proposed method performs quite well in realistic scenarios.

Nevertheless, there are a few limitations of the current method, which we wish to address in our future work. First, the user has to choose the parameter c of the RBF which could potentially affect the results. Typical ways to set this parameter is to use that value for c that minimizes the fitting error in a leave-one-out (or leave-many-out) cross-validation scheme [15]. Second, in this paper, we used a relatively dense sampling scheme, which can be a limiting factor due to long acquisition time. In our future work, we will explore the robustness of this method when very few data samples are available. Further, we will also investigate other potential RBF's which may perform better than the ones used in this work.

Acknowledgements This work has been supported by NIH grants: R01MH097979 (YR), R01MH074794 (CFW), P41RR013218, P41EB015902 and Swedish VR grant 2012-3682(CFW).

References

1. Abramowitz, M.E., et al.: Handbook of Mathematical Functions: with Formulas, Graphs, and Mathematical Tables, vol. 55. Courier Dover, New York (1964)
2. Assaf, Y., Freidlin, R., Rohde, G., Basser, P.: New modeling and experimental framework to characterize hindered and restricted water diffusion in brain white matter. Magn. Reson. Med. **52**(5), 965–978 (2004)
3. Assemlal, H., Tschumperlé, D., Brun, L.: Efficient computation of pdf-based characteristics from diffusion mr signal. In: MICCAI 2008, New York, pp. 70–78 (2008)
4. Barmpoutis, A., Vemuri, B., Forder, J.: Fast displacement probability profile approximation from hardi using 4th-order tensors. In: ISBI, Paris, pp. 911–914 (2008)
5. Buhmann, M.D.: Radial Basis Functions: Theory and Implementations, vol. 12. Cambridge university press, Cambridge/New York (2003)
6. Cohen, Y., Assaf, Y.: High b-value q-space analyzed diffusion-weighted MRS and MRI in neuronal tissues – a technical review. NMR Biomed. **15**(7–8), 516–542 (2002)
7. Descoteaux, M., Deriche, R., Bihan, D., Mangin, J., Poupon, C.: Multiple q-shell diffusion propagator imaging. Med. Image Anal. **15**(4), 603–621 (2011)
8. Ghosh, A., Deriche, R.: Fast and closed-form ensemble-average-propagator approximation from the 4th-order diffusion tensor. In: ISBI, Rotterdam, pp. 1105–1108 (2010)
9. Jensen, J., Helpern, J., Ramani, A., Lu, H., Kaczynski, K.: Diffusional kurtosis imaging: The quantification of non-gaussian water diffusion by means of magnetic resonance imaging. Magn. Reson. Med. **53**(6), 1432–1440 (2005)
10. Merlet, S., Caruyer, E., Deriche, R.: Parametric dictionary learning for modeling eap and odf in diffusion MRI. In: MICCAI, Nice, pp. 10–17 (2012)
11. Moussavi-Biugui, A., Stieltjes, B., Fritzsche, K., Semmler, W., Laun, F.B.: Novel spherical phantoms for q-ball imaging under in vivo conditions. Magn. Reson. Med. **65**(1), 190–194 (2011)
12. Özarslan, E., Koay, C.G., Shepherd, T.M., Komlosh, M.E., İrfanoğlu, M.O., Pierpaoli, C., Basser, P.J.: Mean apparent propagator (map) MRI: a novel diffusion imaging method for mapping tissue microstructure. NeuroImage **78**(2), 16–32 (2013)
13. Piessens, R.: The hankel transform. In: Poularikas, A.D. (ed.) The Transforms and Applications Handbook, 2nd edn., pp. 9–1. CRC, Boca Raton (2000)
14. Rathi, Y., Michailovich, O., Setsompop, K., Bouix, S., Shenton, M., Westin, C.F.: Sparse multi-shell diffusion imaging. In: MICCAI, Toronto, pp. 58–65 (2011)
15. Rippa, S.: An algorithm for selecting a good value for the parameter c in radial basis function interpolation. Adv. Comput. Math. **11**(2–3), 193–210 (1999)
16. Tuch, D., Reese, T., Wiegell, M., Wedeen, V.: Diffusion MRI of complex neural architecture. Neuron **40**, 885–895 (2003)
17. Wedeen, V., Hagmann, P., Tseng, W., Reese, T., Weisskoff, R.: Mapping complex tissue architecture with diffusion spectrum magnetic resonance imaging. Magn. Reson. Med. **54**(6), 1377–1386 (2005)
18. Wu, Y., Alexander, A.: Hybrid diffusion imaging. NeuroImage **36**(3), 617–629 (2007)
19. Ye, W., Portnoy, S., Entezari, A., Vemuri, B.C., Blackband, S.J.: Box spline based 3d tomographic reconstruction of diffusion propagators from MRI data. In: ISBI, Chicago, pp. 397–400. IEEE (2011)
20. Zhang, H., Schneider, T., Wheeler-Kingshott, C.A., Alexander, D.C.: NODDI: Practical in vivo neurite orientation dispersion and density imaging of the human brain. NeuroImage **61**(4), 1000–1016 (2012)